Asia Pacific Academy of Science Pte. Ltd.

Journal of Biological Regulators and Homeostatic Agents 2026, 40(3), 115.
https://doi.org/10.65746/jbrha115

Article

Energy-efficient mixed-mode solar drying using nano-enhanced PCM and desiccant-assisted thermal management for agro-products

Arulraj Ramasamy*, Shanmugam Vangili

Department of Mechanical Engineering, Mahendra Engineering College, Namakkal 637503, Tamil Nadu, India
*** Corresponding author:** Arulraj Ramasamy, arulrajramasamy@outlook.com

CITATION

Ramasamy A, Vangili S. Energy-efficient mixed-mode solar drying using nano-enhanced PCM and desiccant-assisted thermal management for agro-products. Journal of Biological Regulators and Homeostatic Agents. 2026; 40(3): 115.
https://doi.org/10.65746/jbrha115

ARTICLE INFO

Received: 18 April 2026
Revised: 8 May 2026
Accepted: 18 May 2026
Available online: 2 June 2026

Abstract: This study presents an energy-efficient mixed-mode solar drying system integrating nano enhanced thermal storage and desiccant dehumidification to improve the continuous drying of agricultural products. A dual-axis photovoltaic (PV)-powered forced convection dryer was developed and coupled with paraffin wax phase change material (PCM) incorporated with 2 wt% Al_2O_3 nanoparticles and a solar-regenerated bentonite–$CaCl_2$ desiccant bed. Material characterization using SEM, DSC, TGA, and FTIR confirmed stable nanoparticle dispersion, enhanced thermal conductivity, and preservation of chemical integrity within the composite PCM. Drying experiments for turmeric (Curcuma longa) rhizomes were conducted under three modes: (i) forced convection, (ii) forced convection with nano-PCM storage, and (iii) nano-PCM combined with desiccant-assisted dehumidification. The hybrid system significantly reduced drying time, with unsliced turmeric drying in 48, 24, and 22 h, and sliced samples in 36, 18, and 14 h across the respective modes. Compared to traditional open sun drying (95 h), the system improved energy utilization, sustained drying during off-sunshine h, and delivered superior moisture management. The integration of nano-PCM and desiccant technology demonstrated substantial potential for energy recovery, extended operational duration, and improved environmental performance, marking a practical and sustainable solution for post-harvest agro-processing.

Keywords: solar drying; nano-enhanced PCM; thermal energy storage; photovoltaic tracking system; desiccant dehumidification

1. Introduction

Turmeric (Curcuma longa) by Singh, et al. [1] is a traditional medicinal crop that has wide range of pharmacological properties, including antioxidant, anti-parasitic, antitumor, anti-inflammatory, and anti-venom activities [2]. The pharmaceutical industry primarily exploits its bioactive constituents—curcumin, demethoxycurcumin, and bisdemethoxycurcumin —collectively known as curcuminoids, for therapeutic applications [3]. India is the one of the leading producer, consumer, and exporter of turmeric globally. With an estimated cultivation area of 0.32 million hectares, the country yielded 1.16 million tonnes of turmeric, accounting for over 75% of global production in the year 2022–2023. More than thirty distinct varieties grown across diverse agro-climatic regions. The Indian National Turmeric Board projects that turmeric exports will reach a value of USD 1 billion by 2030.

Post-harvest processing of turmeric (Curcuma longa) involves drying to reduce moisture content, which is critical for enhancing shelf life, preserving bioactive constituents, and ensuring storage stability. The selection of an appropriate drying technique plays a vital role in maintaining the quality of curcuminoids and essential oils. Traditionally, open sun drying has been widely adopted due to its simplicity and cost-effectiveness; however, it often results in inconsistent drying, prolonged exposure times, and potential degradation of sensitive compounds. Solar dryers are used to have better quality product and shelf life than conventional open sun drying [4,5]. Various types of solar dryers were developed and tested [6,7]. Among them, indirect forced convection solar dryers [8], offer superior drying efficiency and better-quality retention compared to natural convection systems, though they require electricity for air circulation fans and heaters [9]. To improve energy efficiency, dual axis photovoltaic (PV)-powered forced convection solar dryers are now employed [10,11], reducing dependence on grid electricity while maintaining controlled drying conditions.

Standalone PV module solar dryer by Li, et al. [12] does not work at night. It needs grid power to run the dryer during night time. The weather conditions such as rainy and cloudy days reduce the efficiency of the drying operation. It is necessary to run the dryer throughout the day to attain maximum efficiency. Increase the drying operation time is one of the options to increase the efficiency of dryer.

Integrating a thermal energy storage (TES) unit with a PV-powered solar dryer offers a viable solution for extending drying operations into night time. The TES system stores excess thermal energy during sunlight h and releases it during periods of low or no solar radiation. Phase Change Material (PCM)-based thermal storage [13,14]. is particularly effective for this application due to its high latent heat capacity and isothermal energy release characteristics.

Paraffin wax by Avci and Yazici [15], a widely used PCM, absorbs solar heat during melting and releases it during solidification, maintaining near-constant drying temperatures. Studies on both pure and commercial-grade paraffin wax have demonstrated stable thermal performance over 1030 to 2000 thermal cycles, indicating strong reliability and durability for long-term thermal storage applications in solar drying systems [16].

A low-cost desiccant-assisted solar regenerative drying system by Thoruwa et al. [17] has been demonstrated to contribute 75% of the drying load through hot air and 25% via desiccant dehumidification. A silica gel-based desiccant drying unit was specifically designed for vegetable drying applications [18]. In one study, coarsely chopped coconut pieces were dried using a hot air system integrated with a rotating silica gel desiccant wheel [19]. This system achieved a 25% reduction in drying time compared to conventional hot air drying, due to the lower humidity of the inlet air.

However, the integrated desiccant system showed 40% to 80% higher energy consumption than the standalone hot air system, with approximately 40% of the total energy demand attributed to desiccant regeneration. This highlights the trade-off between enhanced drying efficiency and increased energy input in desiccant-assisted drying technologies.

The main objective of this research work is to evaluate and enhance the performance of a dual axis photovoltaic (PV)-powered solar dryer by integrating it with the nano-metal incorporated phase change materials (PCMs) as thermal storage system and desiccant-based dehumidification units. The study aims to improve thermal storage efficiency using Aluminium Oxide (Al_2O_3) nano particles added PCMs for extended drying during off-sunshine h and enhance moisture removal rates through Bentonite based desiccant-assisted drying, particularly under high humidity conditions. The contributions are:

- Developed a novel mixed-mode solar drying system integrating dual-axis PV-powered forced convection, nano-enhanced PCM thermal storage, and desiccant-assisted dehumidification for continuous agricultural drying.
- Introduced a paraffin wax PCM enhanced with 2 wt% Al_2O_3 nanoparticles, which improved thermal conductivity, heat storage capability, and sustained drying performance during off-sunshine h.
- Combined solar-regenerated bentonite–$CaCl_2$ desiccant technology with nano-PCM storage to achieve superior moisture removal, reduced drying time, and enhanced energy utilization compared with conventional solar drying methods.
- Demonstrated significant improvement in turmeric drying efficiency, reducing drying duration from 95 h in open sun drying to as low as 14 h for sliced samples, while ensuring environmentally sustainable and energy-efficient post-harvest processing.

2. Materials and methods

2.1. Materials

The Erode Variety turmeric was used for drying experiments: Procured from Unjalur, Kodumudi, Tamil Nadu, India (11.1283° N, 77.8772° E).

The solar photovoltaic (PV) system comprised four Luminous polycrystalline solar panels, each rated at 150 Wp with an operating voltage of 12 V. The electrical characteristics of each panel was open-circuit voltage (Voc) of 22 V, short-circuit current (Isc) of 8.9 A, voltage at maximum power (Vmp) of 18.3 V, and current at maximum power (Imp) of 7 A. The panels were constructed with an aluminum frame and had a dimension of 1480 × 680 × 34 mm, weighing 11 kg each. The four panels were connected in parallel to achieve a total capacity of 600 W. A charge controller rated at 40–50 A was used to regulate the power flow from the solar panels to a 12 V, 150 Ah lead-acid battery.

Two stepper motors (Bholanath Precision Engineering Pvt. Ltd.) were employed to drive the solar tracker. Each motor operated at 24–48 V DC with a rated current of 2.8 A, step angle of 1.8°, and holding torque of 3.1 Nm. Each motor weighed approximately 1.4 kg. A 1:20 worm gear transmission was used to facilitate the necessary torque for the tracking system. Air was heated using a flat plate solar collector with gross dimensions of 2.2 × 1.1 × 0.2 m. The absorber consisted of a 1 mm thick aluminum sheet with an absorbing surface area of 2.0 × 1.0 m. The collector was glazed with a single 6 mm thick plain glass cover, spaced 25 mm from the absorber. Insulation materials included polystyrene and silicon rubber for the sides, and 60 mm thick fine wood shavings for the back. Air channels of 20 mm in height facilitated air movement through the collector. Air circulation was achieved using an electric blower (Elmico Power Tools) operating on 230 V and rated at 450 W. The blower provided an airflow of 2.8 m^3/min with adjustable speeds up to 15,000 rpm. A vertical drying chamber was constructed using insulated walls. The chamber measured 0.75 × 0.75 × 1.0 m and housed five drying trays spaced equally. Heated air from the flat plate collector was directed into this chamber for product dehydration. To enable thermal storage, phase change material (PCM) by Aulakh and Joshi [20] in the form of paraffin wax (P1019 grade, ISOCHEM Laboratory Reagent, Angamaly, Kochi) with a melting range of 60–62°C was employed. To enhance the thermal conductivity [21], aluminum oxide (Al_2O_3) nanoparticles (AdNano Technologies Pvt. Ltd., Shivamogga, Karnataka) were used as an additive [22]. The nanoparticles had a purity of ~99%, average particle size.

2.2. Methods

2.2.1. Experimental setup

The integrated experimental setup utilized for the investigation is illustrated in **Figures 1** and **2**. The system includes a dual-axis tracking photovoltaic module equipped with a programmable controller unit and an indirect forced convection solar dryer. The dryer is composed of a fan, a 1 kW centrifugal blower, a flat plate solar air collector, a drying chamber for paraffin wax PCM based on Al_2O_3 nanoparticles, drying trays, and a rooftop desiccant unit. Electrical power for operating the fan and blower is supplied by the dual-axis tracking PV system. For hot air circulation, a single-pass, nonporous flat plate solar air collector was fabricated with dimensions of 1.2 m in width, 2.4 m in length, and 0.2 m in thickness, and is mounted at a fixed angle of 30° facing south. A 6 mm tempered transparent glass cover enhances solar energy transmission to the absorber plate while reducing heat losses. The collector contains a 1 mm thick aluminium absorber plate finished with black matte paint and features a duct height of 0.02 m with adequate thermal insulation. The gap between the glass cover and absorber plate measures 0.025 m, and both are supported by 0.025 m thick wooden frames.

In order to guarantee consistent moisture removal and increased drying efficiency, the drying chamber was built using a forced convection airflow system. A PV-powered fan controlled the airflow, and the desiccant unit improved drying efficiency by lowering air humidity. By taking into account potential measurement errors in temperature, airflow velocity, solar radiation, humidity, and sample weight, an uncertainty analysis was also carried out. The analysis demonstrated the stability and repeatability of the suggested drying method by confirming that the experimental findings were accurate and within acceptable bounds.

Figure 1. Pictorial view of experimental setup.

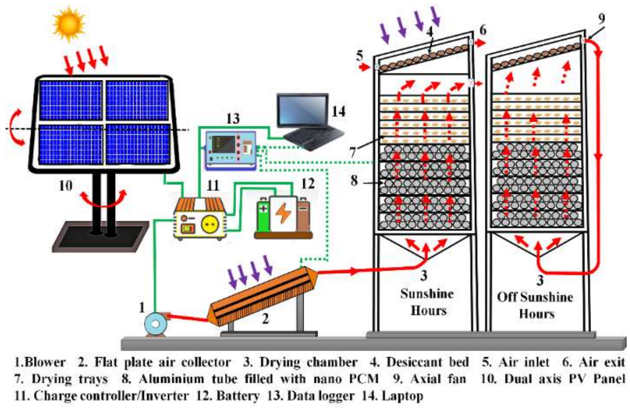

Figure 2. Schematic representation of dual axis PV panel solar dryer setup.

The drying chamber was fabricated with cross-sectional dimensions of 0.75 m × 0.78 m and a height of 1.5 m, using 0.025 m thick marine plywood; the inner walls are insulated with polystyrene for additional thermal retention. The chamber houses twelve trays: the first six are designated for stacking Al_2O_3 nanoparticle-based paraffin wax PCM tubes, while the remaining six hold turmeric rhizomes during drying. The drying chamber rooftop incorporates a 30° slanted bed for regenerative material composed of 60% bentonite, 10% calcium chloride, 20% vermiculite, and 10% cement by dry weight.

The incorporation of 2 wt% Al_2O_3 nanoparticles into paraffin wax significantly enhanced the thermal performance of the PCM by improving its thermal conductivity and heat transfer rate. Faster thermal energy absorption and release were made possible by the enhanced thermal conductivity, which helped to keep the drying temperature steady at times of low solar radiation and off-sunshine. Due to the partial replacement of the base PCM material, the inclusion of nanoparticles somewhat decreased the latent heat storage capacity; however, this decrease was within acceptable bounds and had no negative impact on the total energy storage capacity. The hybrid solar dryer system's higher thermal stability, faster charging and discharging cycles, and increased drying efficiency were the results of the enhanced heat transfer characteristics outweighing the little drop in latent heat.

2.2.2. Working of dual axis solar tracking system (DAST)

The DAST photovoltaic system comprises a PV panel structure, a microcontroller, the Arduino Integrated Development Environment (AIDE) hardware/software, and associated mechanical and electrical components. **Figure 3** shows the Schematic diagram of the dual axis solar tracking PV system.

The PV panel structure consists of three stages: (1) the base structure; (2) the transmission system; and (3) the PV panel fixture. Stage (1): Base Structure The base structure is grouted to the ground and supports stages (2) and (3). It functions as the primary reference during PV panel rotation and is fabricated from mild steel plates with a channel-welded framework. A bearing assembly is incorporated to enable precise rotation about the azimuth axis. Stage (2): Transmission System The transmission system facilitates dual-axis power transmission to track solar movement. The primary rotation defines the azimuth axis, while the secondary rotation defines the altitude angle. This stage includes a pair of gearboxes and a stepper motor assembly designed to achieve positive displacement at minimal speed. A central shaft connects stage (1) to stage (3). The azimuth rotation is controlled by a stepper motor–coupled circular center shaft, while the altitude rotation is controlled by a stepper motor–coupled circular crank plate, which is linked to stage (3) via a pair of connecting elements. Stage (3): PV Panel Fixture and Actuation The system employs two stepper motors, each with a resolution of 1.8° per step, to perform rotational and tilting motions along the azimuth and altitude axes. The motors are driven by specialized driver circuits, which provide the required supply voltage and control signals. Based on commands from the microcontroller, the drivers regulate the stepper motors to rotate in the specified direction and number of steps.

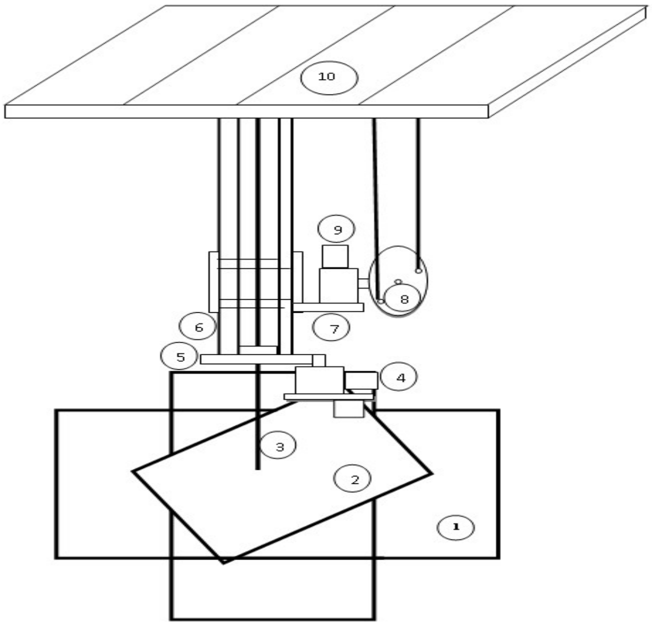

Figure 3. Schematic diagram of the dual axis solar tracking PV system.

1. Base frame. 2. Base plate 3. Center shaft 4. Stepper motor and gear box for azimuth axis 5. Gear wheel 6. Pillar 7. L- Angle plate 8. Crank and mechanical linkage for altitude axis tracking 9. Stepper motor and gear box for altitude axis 10. PV module

2.2.3. Preparation of paraffin wax and Nano-Al_2O_3–n

Table 1 presents the material properties of paraffin wax and Al_2O_3-n. To stabilize the nanocomposite, sodium dodecyl sulfate (SDS) surfactant was employed. The surfactant coats the nanoparticles, effectively preventing aggregation and ensuring uniform dispersion throughout the matrix. To achieve optimal homogeneity, the composite mixture was mechanically stirred at a speed of 1850 rpm for 30 minutes at approximately 80 °C.

Table 1. Paraffin wax and Al2O3properties.

Material	Particle size nm	Density kg/m^3	Melting point °C	Latent heat of fusion kJ/kg	Specific heat capacity kJ/kg.K	Thermal conductivity W/m.K	Purity %
Paraffin wax	-	900	62	253	2.1	0.21	
Al_2O_3	50	600	2072	620	0.955	36	99.7

The resulting nano-phase change material, with a total mass of approximately

108 kg, was subsequently encapsulated inside aluminum tubes with a diameter of 25 mm, wall thickness of 1 mm, and length of 0.74 m. The ends of the tubes were hermetically sealed to completely prevent PCM leakage during phase transition and melting. Each experimental tray accommodated 55 tubes organized in two rows with a zigzag arrangement to maximize packing efficiency and ensure uniform thermal distribution.

2.2.4. Characterization of PCM's

The surface morphology and dispersion of Al_2O_3 nanoparticles within the paraffin wax mixture were examined using Scanning Electron Microscopy (SEM) (**Figure 4**), which revealed the nanoparticle distribution within the composite material. Differential Scanning Calorimetry (DSC) was employed to measure the latent heat and melting point of both pure paraffin wax (PW) and the Al_2O_3–paraffin wax (PW-n) phase change material (PCM) [23,24]. This technique enables the identification of changes in melting behavior or thermal properties induced by the incorporation of nanoparticles. Thermogravimetric analysis (TGA) was performed to evaluate the weight loss percentage of PW and PW-n as a function of temperature, thereby providing insights into the thermal stability and decomposition characteristics of the nanocomposite material. Finally, Fourier Transform Infrared Spectroscopy (FTIR) was used to analyze the chemical composition of the PW and PW-n, providing information on any alterations in bonding or functional groups attributable to the nanoparticles.

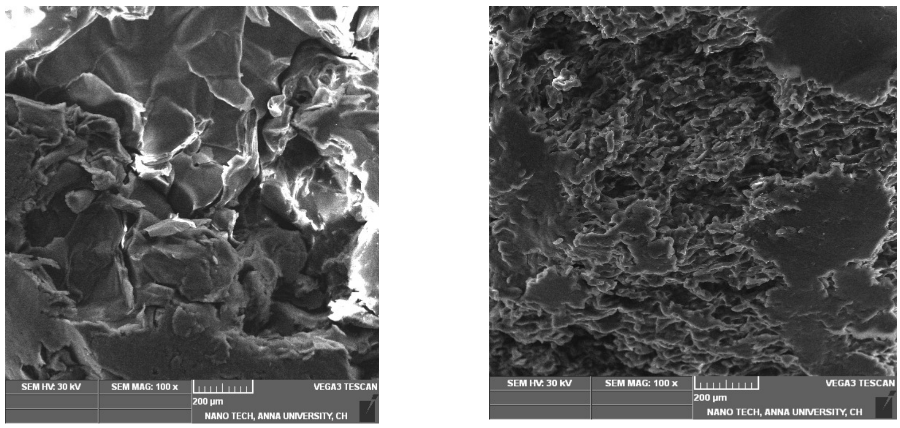

(a) **(b)**

Figure 4. SEM scanned images of pure paraffin wax and Paraffin Wax blended with 2% Al_2O_3 nanoparticle. **(a)** Pure paraffin wax; **(b)** Paraffin wax with 2%AL_2O_3 nanoparticle.

2.2.5. Experimental procedure

Solar drying experiments were conducted to study the drying behavior of turmeric rhizomes under three distinct modes: (i) forced convection; (ii) forced convection with Al_2O_3 nanoparticle paraffin wax phase change material (PCM); and (iii) forced convection with Al_2O_3 nanoparticle paraffin wax PCM combined with a solid desiccant bed. The experiments were performed at Vazhakuttapatti, Tamil Nadu, India (11.601926° N, 77.876230° E). Farm-fresh turmeric rhizomes were collected from local farmers and thoroughly washed in running water to remove dirt and impurities. Subsequently, the rhizomes were cured by boiling in hot water at 100 °C for 45 minutes, which softens the rhizomes and ensures more uniform drying. For each trial, 30 kg of cured turmeric rhizomes were loaded onto six trays.

The mass flow rate of air through the flat plate collector was maintained at 0.02 $kg \cdot m^{-2} \cdot s^{-1}$ during sunlight h and reduced to 0.005 $kg \cdot m^{-2} \cdot s^{-1}$ during cloudy or post-sunset conditions. Each experimental run commenced at 09:00 IST and concluded at 17:00 IST. After sunshine h, the drying process continued using heat stored in the PCM.

2.3. Drying characteristics

Turmeric samples were dried in an oven at 105 °C for 24 h to assess their moisture content. Equilibrium moisture content was calculated using a mechanical dryer at 60 °C until no mass change occurred. Moisture, drying rate and moisture ratio of turmeric rhizomes is evaluated using the following equations [25–27].

Initial moisture content

$$M_{wb} = \frac{W_o - W_d}{W_o} \tag{1}$$

Final moisture content

$$M_f = \frac{W_{wet} - W_d}{W_d} \tag{2}$$

The drying rate is evaluated by using

$$M_t = \frac{W - W_s}{W_s} \qquad \frac{\text{kg total moisture}}{\text{kg dry solid}} \tag{3}$$

W - mass of fresh turmeric (kg); Ws- mass of dry solid (kg)

Moisture ratio

$$MR = \frac{M_t - M_{eq}}{M_o - M_{eq}} \tag{4}$$

The nano-enhanced PCM was prepared by dispersing 2 wt% Al_2O_3 nanoparticles into molten paraffin wax using a controlled two-step preparation method to ensure uniform particle distribution and stable thermal performance. Initially, the nanoparticles were mechanically stirred with the melted paraffin wax at a constant temperature, followed by ultrasonication for several h to minimize particle agglomeration and improve dispersion stability within the PCM matrix. The sonication process enhanced the interaction between nanoparticles and the base material, resulting in improved thermal conductivity and heat transfer characteristics. To evaluate long-term stability, the composite PCM was subjected to repeated thermal charging–discharging cycles, and its structural and chemical stability were examined using SEM, DSC, FTIR, and TGA analyses. The results confirmed stable nanoparticle dispersion, negligible phase separation, consistent thermal storage behavior, and preservation of chemical integrity even after prolonged thermal cycling, demonstrating the suitability of the nano-PCM for continuous solar drying applications.

2.4. Statistical parameters

2.4.1. Thermal efficiency

The thermal efficiency of the solar dryer is expressed as:

$$\eta_{th} = \frac{m_w L_v}{IAt} \times 100 \quad (5)$$

Where, η_{th} = thermal efficiency (%), m_w = mass of evaporated moisture (kg), Lv = latent heat of vaporization (kJ/kg)

2.4.2. Specific energy consumption (SEC)

The specific energy consumption is calculated as:

$$SEC = \frac{E_{total}}{m_w} \quad (6)$$

Where: SEC = specific energy consumption (kWh/kg), E_{total} = total energy consumed (kWh), m_w = moisture removed (kg)

2.4.3. Effective moisture diffusivity

The effective moisture diffusivity is determined using Fick's diffusion equation:

$$MR = \frac{8}{\pi^2} \exp\left(\frac{-\pi^2 D_{eff} t}{4L^2}\right) \quad (7)$$

Where, MR = moisture ratio, D_{eff} = effective moisture diffusivity (m^2/s), t = drying time (s), L = half thickness of sample (m).

3. Results and discussion

The article primarily presents experimental findings about the drying and thermal performance of the suggested hybrid solar dryer in various operating modes. The findings show that the combination of desiccant-assisted dehumidification and nano-enhanced PCM promoted heat retention, decreased chamber humidity, and maintained continuous drying during off-sun h. Both sliced and unsliced turmeric samples showed notable drying time reductions as compared to traditional forced convection and open sun drying techniques. The hybrid system's efficacy for energy-efficient and sustainable agricultural drying applications was confirmed by the results, which also demonstrated increased thermal efficiency, decreased specific energy consumption, improved exergy utilization, and faster moisture diffusion rates.

3.1. Morphology and microstructure analysis

The morphology and microstructure of PW, and PW-n (2% Al_2O_3 nanoparticles) are shown in **Figure 4**. The SEM micrographs reveal that the nanocomposite exhibits a sponge-like structure with irregularly shaped particles. Al_2O_3 nanoparticles are dispersed throughout the paraffin matrix in varying proportions. The size and shape of the particles depend on the concentration of alumina; as the weight percentage of Al_2O_3 increases, the average particle size also increases. Additionally, higher nanoparticle weight percentages lead to increased aggregation, which consequently reduces fluidization. This morphology is indicative of a modified thermal conductivity profile, which could enhance the performance of the PCM for thermal energy storage applications.

3.2. Thermal stability and phase change characteristics

The effects of adding Al_2O_3 nanoparticles to paraffin wax on thermal stability were investigated using Differential Scanning Calorimetry (DSC) and Thermogravimetric Analysis (TGA). Heat flow curves obtained from DSC (**Figures 5** and **6**) illustrate the temperature characteristics of both PW and PW-n.

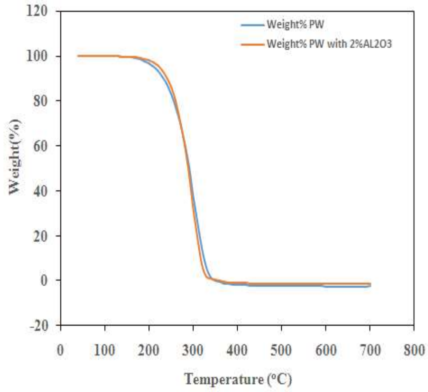

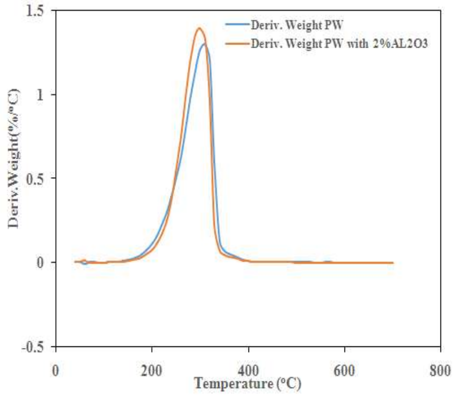

(a) **(b)**

Figure 5. TGA curve for PW and PW with nano-PCM. **(a)** TGA curve of pure paraffin wax (PW); **(b)** TGA curve of paraffin wax containing 2 wt% Al_2O_3 nanoparticles (PW-n).

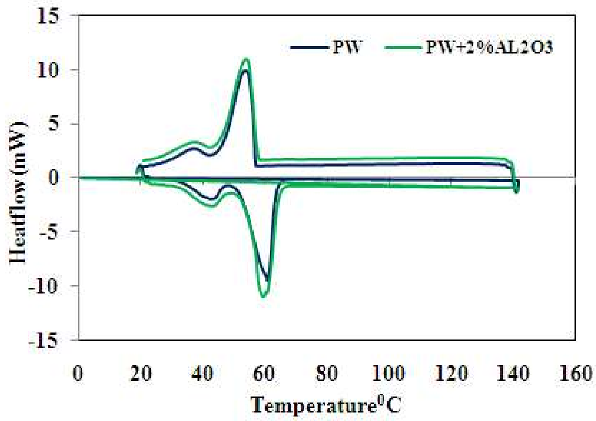

Figure 6. DSC curve for PW with PW + nano-PCM.

The DSC results show that the addition of nanoparticles does not significantly alter the phase transition properties. An endothermic peak during melting is observed in both PW and PW-n, indicating the presence of isomorphous crystalline structures. Similarly, exothermic peaks during solidification confirm crystallization in all samples. The heat transfer during the liquid-to-solid phase occurs at nearly constant temperature, attributed to efficient convective heat transfer in the liquefaction phase, with excess heat rejected upon complete solidification. The optimum degradation temperature (ODT), derived from the first derivative of mass loss with respect to temperature, indicates the temperature at which the material experiences the maximum degradation rate. For PW, the ODT is 310 °C (DTG – 1.4% / °C), and for PW + nano-

PCM. It is slightly lower at 300 °C (DTG - 1.3% / °C) [28–30]. This suggests that the thermal stability is maintained upon nanoparticle addition. Overall, the thermal conductivity enhancement from Al_2O_3 nanoparticles accelerates heat transfer without compromising the phase transition behavior or thermal stability of paraffin wax PCM.

3.3. FTIR analysis

The FTIR study demonstrates no significant differences in wavelength peaks between PW and PW-n PCM samples, as shown in **Figures 7a, b**. PW, primarily composed of CH_2 and CH_3 groups, has the chemical formula $C_{28}H_{58}$. Characteristic peaks at 2911 and 2844 cm^{-1} correspond to asymmetric and symmetric stretching vibrations of CH_2 and CH_3 molecules, respectively. Two weak but sharp peaks at 1463 and 722 cm^{-1} are attributed to in-plane and out-of-plane bending modes of CH_3 groups. In the PW-n, similar peaks appear at 1461 cm^{-1} and 718 cm^{-1}, indicating the presence of bonding interactions between nanoparticles and the paraffin matrix. Importantly, these findings suggest that the Al_2O_3 nanoparticles physically interact with the paraffin wax without altering its chemical structure, thereby preserving the chemical stability of the composite material upon nanoparticle incorporation.

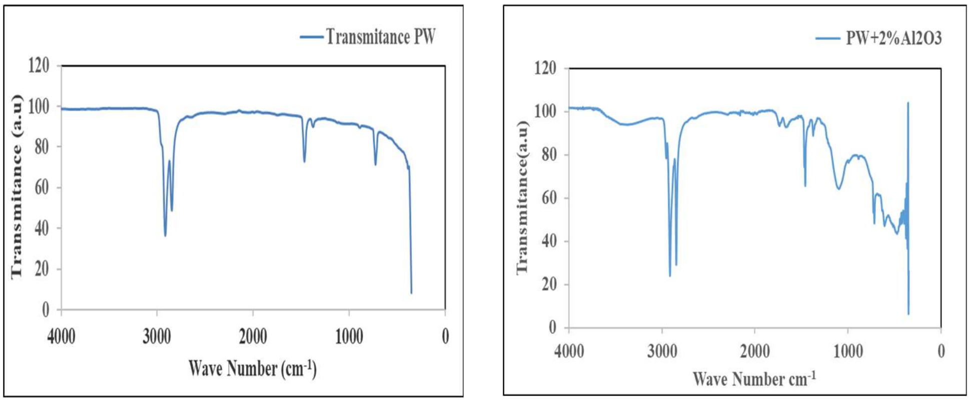

Figure 7. FTIR Spectra for PW and PW-n. **(a)** Pure paraffin wax (PW); **(b)** Paraffin wax containing 2 wt% Al_2O_3 nanoparticles (PW-n).

3.4. Drying characteristics of turmeric rhizomes

Turmeric rhizomes with an initial moisture content of approximately 87.5% (wet basis) were dried to a final moisture content of 8% using three different drying modes. Open sun drying required about 95 h for unsliced rhizomes and 58 h for sliced rhizomes to reach the target moisture level. Moisture variation with drying time is shown in **Figures 8** and **9**.

For unsliced turmeric rhizomes, drying times were 48 h, 24 h, and 22 h for drying modes (i), (ii), and (iii), respectively. The integration of PCM and a desiccant in the post sunshine h resulted in significant improvements, reducing the drying time by approximately one day. For sliced turmeric, the equilibrium moisture content was reached in 36 h, 18 h, and 14 h respectively in modes (i), (ii), and (iii). These results suggest that slicing the rhizomes accelerates drying due to the increased surface area exposed to the drying environment, facilitating faster moisture removal. Additionally, the combined use of PCM storage and desiccant beds further enhances drying efficiency by providing additional moisture removal mechanisms and better temperature regulation. These findings are consistent with earlier research. **Figure 10** shows that the drying rate varies throughout the process, progressively decreasing as the turmeric rhizome approaches equilibrium moisture content. The drying occurs entirely during the falling rate period, characterized by an initial rapid drying phase followed by a steady slowdown. The absence of a constant rate drying period underscores the dominance of the falling rate period in the drying kinetics of turmeric rhizomes.

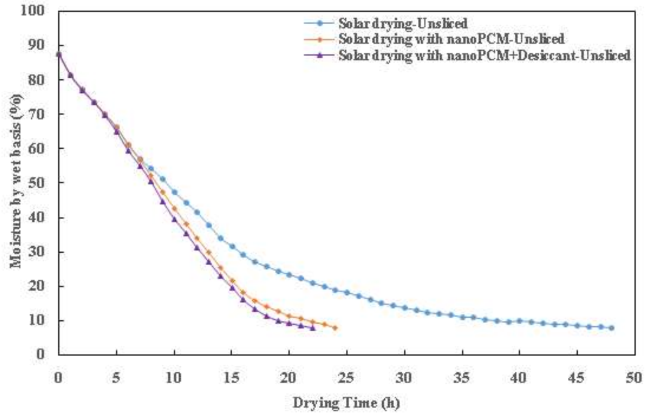

Figure 8. Variation of moisture content vs drying time (Unsliced).

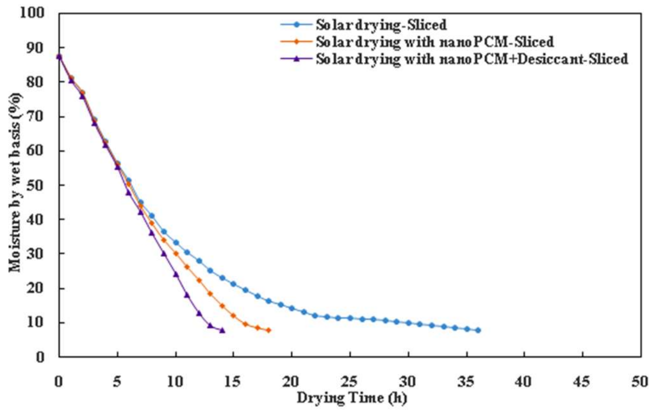

Figure 9. Variation of moisture content vs drying time (Sliced).

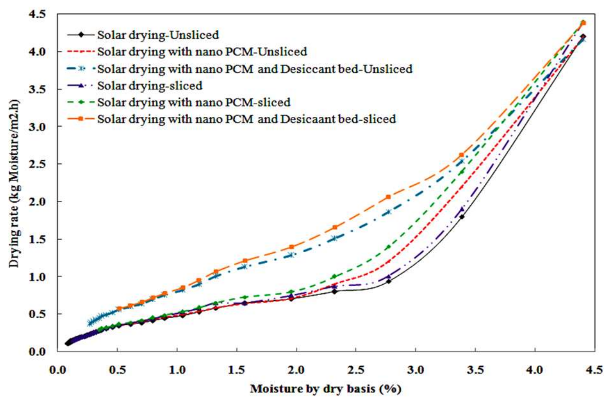

Figure 10. Variation of moisture content vs drying time.

The results may not be applicable to other agricultural products and surroundings because the study is restricted to experimental validation under particular meteorological conditions and turmeric drying applications. Further research is also needed on the long-term economic viability, large-scale industrial application, and durability evaluation of nano-PCM and desiccant materials.

4. Conclusion

The study demonstrates that integrating dual-axis photovoltaic tracking, Al_2O_3 nanoparticle enhanced paraffin PCM, and a solar-regenerated desiccant bed significantly enhances the performance of mixed-mode solar drying systems for high-moisture agricultural produce. Structural and thermal characterization validated that nano-additives improved PCM heat transfer without compromising phase transition behavior or chemical stability. Experimental results revealed substantial reductions in drying time for turmeric rhizomes compared to both open sun and conventional forced convection drying. The hybrid system ensured continuous drying beyond sunshine h, improved energy utilization, decreased humidity levels, and maintained stable thermal conditions. The combined effect of thermal energy storage and desiccant-assisted moisture removal positions the mixed-mode system as a reliable, sustainable, and energy-efficient technology. This approach is scalable to various agro-products and contributes to improved energy recovery, better resource utilization, and enhanced environmental performance in rural and decentralized processing sectors. To improve automation, scalability, and industrial applicability of the suggested solar drying system, further work might incorporate real-time IoT monitoring, AI-based intelligent drying control, predictive energy management, and thorough techno-economic feasibility analysis.

Author contributions: Conceptualization, AR and SV; methodology, AR; software, AR; validation, AR and SV; formal analysis, SV; investigation, SV; resources, AR; data curation, SV; writing—original draft preparation, AR; writing—review and editing, AR; visualization, SV; supervision, SV; project administration, SV; funding acquisition, SV. All authors have read and agreed to the published version of the manuscript.

Funding: None.

Ethical approval: Not applicable.

Informed consent statement: Not applicable.

Conflict of interest: The authors declare no conflict of interest.

References

1. Singh G, Kapoor IPS, Singh P, et al. Comparative study of chemical composition and antioxidant activity of fresh and dry rhizomes of turmeric (Curcuma longa Linn.). Food and Chemical Toxicology. 2010; 48(4): 1026–1031. doi: 10.1016/j.fct.2010.01.015
2. Ravindran PN, Babu KN, Sivaraman K. Turmeric: the genus Curcuma. CRC Press; 2007.
3. Saha G, Sharangi AB, Upadhyay TK, et al. Dynamics of drying turmeric rhizomes (Curcuma longa L.) with respect to its

moisture, color, texture and quality. Agronomy. 2022; 12(6): 1420. doi: 10.3390/agronomy12061420
4. Singh D, Mall P. Experimental investigation of thermal performance of indirect mode solar dryer with phase change material for banana slices. Energy Sources, Part A: Recovery, Utilization, and Environmental Effects. 2024; 46(1): 15268–15285. doi: 10.1080/15567036.2020.1810825
5. Singh P, Gaur MK. Review on development, recent advancement and applications of various types of solar dryers. Energy Sources, Part A: Recovery, Utilization, and Environmental Effects. 2024; 46(1): 14471–14491. doi: 10.1080/15567036.2020.1806951
6. Borah A, Hazarika K, Khayer SM. Drying kinetics of whole and sliced turmeric rhizomes (Curcuma longa L.) in a solar conduction dryer. Information Processing in Agriculture. 2015; 2(2): 85–92. doi: 10.1016/j.inpa.2015.06.002
7. Lokeswaran S, Eswaramoorthy M. Experimental studies on a solar drier system with a biomass back-up heater. Energy Sources, Part A: Recovery, Utilization, and Environmental Effects. 2013; 35(5): 467–475. doi: 10.1080/15567036.2010.511434
8. Lakshmi DVN, Muthukumar P, Layek A, et al. Performance analyses of mixed mode forced convection solar dryer for drying of stevia leaves. Solar Energy. 2019; 188: 507–518. doi: 10.1016/j.solener.2019.06.009
9. Ekechukwu OV, Norton B. Review of solar-energy drying systems II: An overview of solar drying technology. Energy Conversion and Management. 1999, 40(6): 615–655. doi: 10.1016/s0196-8904(98)00093-4
10. Hafez AZ, Yousef AM, Harag NM. Solar tracking systems: Technologies and trackers drive types–A review. Renewable and Sustainable Energy Reviews. 2018; 91: 754–782. doi: 10.1016/j.rser.2018.03.094
11. Fathabadi H. Comparative study between two novel sensorless and sensor based dual-axis solar trackers. Solar Energy. 2016; 138: 67–76. doi: 10.1016/j.solener.2016.09.009
12. Li G, Tang R, Zhong H. Optical performance of horizontal single-axis tracked solar panels. Energy Procedia. 2012; 16: 1744–1752. doi: 10.1016/j.egypro.2012.01.270
13. Esen M, Ayhan T. Development of a model compatible with solar assisted cylindrical energy storage tank and variation of stored energy with time for different phase change materials. Energy Conversion and Management. 1996; 37(12): 1775–1785. doi: 10.1016/0196-8904(96)00035-0
14. Rehman HU, Naseer F, Ali HM. An experimental case study of solar food dryer with thermal storage using phase change material. Case Studies in Thermal Engineering. 2023; 51: 103611. doi: 10.1016/j.csite.2023.103611
15. Avci M, Yazici MY. Experimental study of thermal energy storage characteristics of a paraffin in a horizontal tube-in-shell storage unit. Energy conversion and Management. 2013; 73: 271–277. doi: 10.1016/j.enconman.2013.04.030
16. Samara H, Hamdan M, Al-Oran O. Effect of Al2O3 nanoparticles addition on the thermal characteristics of paraffin wax. International Journal of Thermofluids. 2024; 22: 100623. doi: 10.1016/j.ijft.2024.100623
17. Thoruwa TFN, Johnstone CM, Grant AD, et al. Novel, low cost CaCl2 based desiccants for solar crop drying applications. Renewable Energy. 2000; 19(4): 513–520. doi: 10.1016/s0960-1481(99)00072-5
18. Nagaya K, Li Y, Jin Z, et al. Low-temperature desiccant-based food drying system with airflow and temperature control. Journal of Food Engineering. 2006; 75(1): 71–77. doi: 10.1016/j.jfoodeng.2005.03.051
19. Madhiyanon T, Adirekrut S, Sathitruangsak P, et al. Integration of a rotary desiccant wheel into a hot-air drying system: Drying performance and product quality studies. Chemical Engineering and Processing: Process Intensification. 2007; 46(4): 282–290. doi: 10.1016/j.cep.2006.06.008
20. Aulakh JS, Joshi DP. Thermal and morphological study of paraffin/SEBS/expanded graphite composite phase change material for thermal energy storage. Energy Sources, Part A: Recovery, Utilization, and Environmental Effects. 2022; 44(1):

986–1003. doi: 10.1080/15567036.2022.2053764

21. Bahari M, Najafi B, Babapoor A. Evaluation of α-AL2O3-PW nanocomposites for thermal energy storage in the agro-products solar dryer. Journal of Energy Storage, 2020; 28: 101181. doi: 10.1016/j.est.2019.101181
22. Manoj Kumar P, Mylsamy K, Saravanakumar PT. Experimental investigations on thermal properties of nano-SiO2/paraffin phase change material (PCM) for solar thermal energy storage applications. Energy Sources, Part A: Recovery, Utilization, and Environmental Effects. 2020; 42(19): 2420–2433. doi: 10.1080/15567036.2019.1607942
23. Akgun M, Aydin O, Kaygusuz K. Thermal energy storage behavior of a paraffin during melting and solidification. Energy Sources, Part A. 2007; 29(14): 1315–1326. doi: 10.1080/00908310600710681
24. Rao ZH, Zhang GQ. Thermal properties of paraffin wax-based composites containing graphite. Energy Sources, Part A: Recovery, Utilization, and Environmental Effects. 2011; 33(7): 587–593. doi: 10.1080/15567030903117679
25. Chokngamvong S, Suvanjumrat C. Study of drying kinetics and activation energy for drying a pineapple piece in the crossflow dehydrator. Case Studies in Thermal Engineering. 2023; 49: 103351. doi: 10.1016/j.csite.2023.103351
26. Ray A, Mohanty S, Jena S, et al. Drying methods affects physicochemical characteristics, essential oil yield and volatile composition of turmeric (Curcuma longa L.). Journal of Applied Research on Medicinal and Aromatic Plants. 2022; 26: 100357. doi: 10.1016/j.jarmap.2021.100357
27. Abubakar S, Umaru S, Kaisan MU, et al. Development and performance comparison of mixed-mode solar crop dryers with and without thermal storage. Renewable Energy. 2018; 128: 285–298. doi: 10.1016/j.renene.2018.05.049
28. Bui TH, Tien Nguyen G. Enhanced thermal energy storage of n-octadecane-impregnated mesoporous silica as a novel shape-stabilized phase change material. ACS Omega. 2022; 7(14): 12222–12230. doi: 10.1021/acsomega.2c00623
29. Prasad AK, Singh DK, Shankar R. Performance analysis of heating and humidification system with solar assisted CaCl2 desiccant wheel rotor. Energy Sources, Part A: Recovery, Utilization, and Environmental Effects. 2022; 44(4): 9086–9102. doi: 10.1080/15567036.2022.2128941
30. Tiwari S, Tiwari G N. Energy and exergy analysis of a mixed-mode greenhouse-type solar dryer, integrated with partially covered N-PVT air collector. Energy. 2017; 128: 183–195. doi: 10.1016/j.energy.2017.04.022